Plasmonics (2025) 20:7873–7881
https://doi.org/10.1007/s11468-025-02820-z

RESEARCH

Design of an Advanced Sensor Based on Surface Plasmon Resonance with Ultra-High Sensitivity

H. Bouandas[1] · Y. Slimani[2] · Malek G. Daher[3] · A. Djemli[4,5] · M. Fatm[6] · Samar A. Aldossari[7] · Mika Sillanpää[8,9,10,11]

Received: 7 January 2025 / Accepted: 3 February 2025 / Published online: 18 February 2025

Abstract

This study presents the development of a high-sensitivity surface plasmon resonance (SPR) sensor featuring an innovative structure composed of a BK7 prism glass, copper (Cu) thin film, titanium dioxide (TiO_2), nickel (Ni), and a two-dimensional black phosphorus (BP) layer combined with a sensing medium. The sensor utilizes an angular interrogation technique, with its performance parameters sensitivity (S), detection accuracy (DA), and quality factor (QF) analyzed using the attenuated total reflection (ATR) and transfer matrix method (TMM). The results demonstrate significant improvements in the full-width at half-maximum (FWHM), detection accuracy, quality factor, and sensitivity due to the hybrid TiO_2, Ni, and BP layers. The impact of copper thickness is also thoroughly investigated. The study identifies optimal sensor performance with a sensitivity of 518°/RIU and a quality factor of 91.51/RIU, achieved with optimized thicknesses of 35 nm (Cu), 2×4 nm (TiO_2), 10 nm (Ni), and 0.53 nm (BP). Furthermore, an alternative configuration yields even higher sensitivity, achieving 526°/RIU and a quality factor of 96.51/RIU, with a copper thickness of 35 nm, TiO_2 thickness of 2×2 nm, and nickel thickness of 15 nm. The enhanced sensitivity and performance of the TiO_2, Ni, and BP hybrid layers suggest their promising applicability in diverse biosensing scenarios. This study highlights the potential of this optimized SPR sensor configuration for advanced biosensing applications, owing to its high sensitivity and improved quality factor.

Keywords High-sensitivity · SPR sensor · BK7 prism glass · BP hybrid layer

Introduction

Because of their unique features, high sensitivity to changes in the refractive index near the sensor surface, fast detection capability in real time, quick response, and hold great potential for use in biomedical research surface plasmon resonance (SPR) sensors have attracted much attention [1]. Recent advancements in SPR sensor designs have significantly improved sensitivity and specificity across various applications. A multilayer sensor with PVP, Ag–Ni, and ZnS

✉ M. Fatm
fatmimessaoud@yahoo.fr

1 Applied Optics Laboratory, Institute of Optics and Precision Mechanics, University Setif 1, 19000 Setif, Algeria

2 Laboratory of Intelligent System, Faculty of Technology, University Ferhat Abbas Setif 1, 19000 Setif, Algeria

3 Physics Department, Islamic University of Gaza, P.O. Box 108, Gaza, Palestine

4 Faculty of Physics, University of Sciences & Technology Houari Boumediene (U.S.T.H.B), BP 32, El Alia, Bab Ezzouar 16111, Algiers, Algeria

5 Physics and Chemistry of Materials Lab, Department of Physics, University Mohamed Boudiaf of M'sila, M'sila 28000, Algeria

6 Research Unit On Emerging Materials (RUEM), University Ferhat Abbas of Setif 1, 19000 Setif, Algeria

7 Department of Chemistry, College of Sciences, King Saud University, P.O. Box 2425, Riyadh, Saudi Arabia

8 Department of Biological and Chemical Engineering, Aarhus University, Norrebrogade 44, 8000 Aarhus, Denmark

9 Saveetha School of Engineering, Saveetha Institute of Medical and Technical Sciences, Saveetha University, Chennai, Tamil Nadu 602105, India

10 Functional Materials Group, Gulf University for Science and Technology, Mubarak Al-Abdullah, 32093 Kuwait, Kuwait

11 Centre of Research Impact and Outcome, Chitkara University Institute of Engineering and Technology, Chitkara University, Rajpura 140401, Punjab, India

layers achieved a sensitivity of 252.5°/RIU for petrochemical detection. In cancer diagnostics, an Fe_2O_3-CNT sensor with Ag-Pt layers demonstrated exceptional sensitivity of 320.571°/RIU and a FoM of 174.129 RIU^{-1} for MCF-7 cells [2, 3]. Another sensor employing CNT and graphene, optimized using machine learning, reached 340.44°/RIU sensitivity for formalin detection. For hemoglobin detection, a five-layered SPR sensor with ZnO nanowires and graphene achieved 207°/RIU sensitivity. Finally, a perovskite/Si-based SPR sensor using $KSnI_3$ demonstrated superior performance with 348.75°/RIU sensitivity and broad applicability for chemical sensing. These developments underscore the critical role of material innovation in advancing SPR technologies for diverse fields [4, 5].

SPR has shown to be a very effective optical technology method for accurately determining the size of viruses or cells. Plasmonic nanostructures can be accurately manipulated and controlled by SPR-based techniques, facilitating the development of advanced photonic devices, sensors, and optoelectronic components with tailored optical properties [6]. Two coupling configurations are commonly used in SPR prisms: the Otto configuration [7] and the Kretschmann configuration [8]. For excitation of a strongly localized exponentially fading evanescent wave, the most widely used coupling is the Kretschmann configuration. Through surface plasmons (SPs), the evanescent wave is generated across the interface, a collective oscillation the charge density of free electrons, which are produced in SPR sensors during light contact between dielectric and metal, specifically gold, silver, and copper. The resonance conditions, including the resonance angle, wavelength, and intensity of the reflected light, are considerably changed by this wave, which is highly influenced by the various in the surrounding RI [9–11]. A lot of recent research favored Copper (Cu) as the second most conductive material after silver, which is far less expensive than both gold and silver. Cu has not gotten much attention as a plasmonic material because of how quickly and easily it oxidizes metal [12]. Appropriate oxide coatings can stop copper from oxidizing, according to recent research by Singh et al. [13].

Innovative SPR sensor designs have been developed to achieve high sensitivity and performance across various applications. One design utilized a $TiSi_2$-BP structure for cancer cell detection, achieving a sensitivity of 218.6°/RIU [14, 15]. Another sensor based on MXene, graphene, and ZnO layers demonstrated 161°/RIU sensitivity for hemoglobin detection. For dopamine detection, an SPR sensor employing ZnO nanowires and cerium oxide achieved a sensitivity of 95°/RIU. In chemical sensing, a ZnO-Si-Ag sensor achieved a sensitivity of 311°/RIU [16, 17]. It has a sensitivity of up to 502°/RIU and a figure of merit (FoM) of 128.7RIU-1. Cu/BaTiO3/BP structures show exceptionally high sensitivity of 378°/RIU, according to Karki et al. [18]. For organic compound detection, a WTe_2-based sensor reached a sensitivity of 213.75°/RIU. In cancer diagnostics, a sensor using Au–Ag alloys and WS_2 layers achieved 304°/RIU sensitivity and a penetration depth of 189.79 nm. Finally, a long-range SPR (LRSPR) sensor with a 2S2G/Cu/Graphene configuration achieved 4655.7°/RIU imaging sensitivity for bacterial detection. These advancements highlight the importance of innovative materials and configurations in enhancing sensor performance [19–21].

Vibisha et al. had suggested that the SPR sensor's sensitivity could be even higher due to the bimetallic layer of Cu and Ni. They demonstrated that the Cu–Ni–WS2 configuration can achieve a sensitivity of 480 °/RIU [22]. To date, black phosphorus (BP), a recently found new 2D material employed in the SPR sensor, has drawn interest due to its large molar response factor, low extinction, direct bandgap high mobility, quick biomolecular adsorption energy, and low absorption. Even though BP oxidizes quickly, adding another material produces low oxidation because molecule binding is effective inside the sensing layer [23, 24]. It has been demonstrated that combining BP with bilayer WSe2 on a BK7 prism improves sensitivity to 279°/RIU [25]. A sensitivity 348.75°/RIU was attained when using few-layer perovskite materials with Cu [26]. Kumar, Rajeev et al. Using the angular interrogation method, the Cu-Ni layer with BP commuted the highest sensitivity of 525°/RIU at a wavelength of 633 nm [27]. BP has also been seen in research in sensor applications, optoelectronics, and electronic field [28], due to the exceptional properties of titanium dioxide (TiO_2) such as its good chemical stability, wide range of features, and wide band gap, including a high dielectric constant and a high dielectric constant [29]. One material that shows promise for use in sensor devices is TiO_2 [30]. The sensitivity of SPR sensors is increased at the interface due to field enhancement caused by the relatively high dielectric constant of a TiO_2 layer deposited on a metal [31]. Mostufa et al. have been proposed BK7/TiO_2/Au/graphene for improving the sensitivity up to 292.857 deg/RIU [32]. TiO_2 is a common material used in sensors, and 210.75 degree/RIU is the highest sensitivity that has been attained [33]. The maximum sensitivity value of 502 (0/RIU) was obtained by Shivam Singh et al. [34], using an SPR biosensor based on BK7/TiO_2/Au/graphene for the detection of SARS-CoV-2. A SPR sensor using TiO_2/Ag/MoSe2/Graphene film design and numerically enhanced the sensitivity above 194°/RIU was demonstrated by Moznuzzaman et al. [35].

In this numerical work, we have designed and analyzed the detection performance parameters for a new configuration of a highly sensitive SPR sensor using the structure (BK7/Cu/TiO_2/Ni/BP). Numerical transfer matrix simulations were employed in our suggested SPR sensor. In this case, the sensor performance was enhanced by the addition

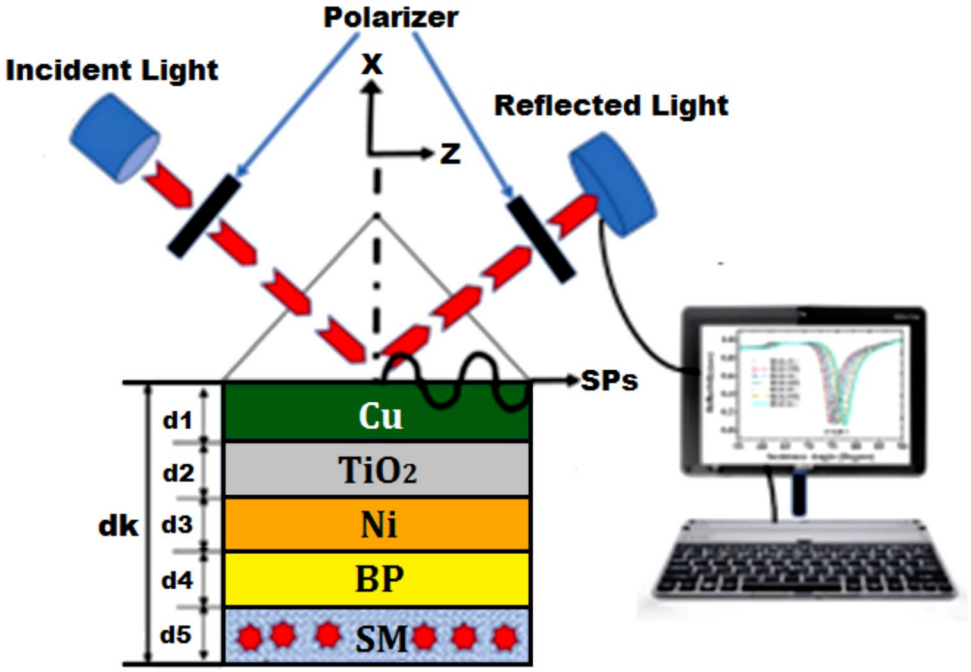

Fig. 1 Structure of the suggested SPR sensor

of TiO_2, Ni, and 2D material (BP). The parameters will be fine-tuned to achieve maximum sensitivity and high QF while also achieving enhanced sensitivity and minimum reflectance. These are arranged as follows: the "Theoretical Model" section presents the mathematical framework and theoretical model. A thorough discussion and a description of the results were provided in the "Results and Discussion" section. Finally, the "Conclusion" section concludes the article.

Theoretical Model

Structure of Proposed Sensor

The proposed sensor having five layers BK7 prism, copper (Cu), titanium dioxide (TiO_2), nickle (Ni), and black phosphor (BP). The sensing medium will take 1.330 and 1.335. The thicknesses of Cu, TiO_2, Ni, and BP layers are indicated as d_1, d_2, d_3, and d_4, and the refractive indices are showed as n_1, n_2, n_3, and n_4, respectively. The refractive index (RI) of two metals, copper (Cu) and nickel (Ni), can be expressed as follows [36, 37]:

$$\varepsilon_{Cu} = 1 - \lambda^2 \lambda_c / \left[{\lambda_p}^2 \left(\lambda_c + i\lambda \right) \right] \quad (1)$$

Here, $\lambda_c = 4.0852 \times 10^{-5}$ m and $\lambda_p = 1.3617 \times 10^{-7}$ m represent the wavelength of collision and the plasma of copper, for Ni, $\lambda_p = 2.8409 \times 10^{-5}$ m and $\lambda_p = 2.5381 \times 10^{-7}$ m, respectively.

Table 1 The ideal material thickness and refractive index for the current sensor are 633 nm

Material	Thickness of monolayer (nm)	Refraction index	Ref
Prism BK7	–	1.5151	[38]
Cu	35–65	0.0369 + 4.5393i	[36]
`TiO_2	L*2	2.5837	[39]
Ni	5–15	0.0303 + 2.2843i	[37]
BP	0.53	3.5 + 0.01i	[40]

The analysis is based on MATLAB simulation. Figure 1 shows the recommended SPR sensor based on layers of Cu, TiO_2, Ni, and BP layers schematically. Table 1 presents the refractive index (RI) values and thicknesses for all layers of the suggested sensor.

Reflectance

The transfer matrix technique (TMT) for the N-layer structure has been exploited to calculate the reflectance of the SPR sensor. Along the *z*-axis, all of the layers are arranged. Mathematically, first limit ($z = 0$) and last limit ($z = z_{N-1}$) tangential fields are associated as [41].

$$\begin{bmatrix} E_1 \\ M_1 \end{bmatrix} = G \begin{bmatrix} E_{N-1} \\ M_{N-1} \end{bmatrix} \quad (2)$$

where the electric tangential fields at the first limit and the last limit, respectively, are E_1 and E_{N-1}. The magnetic tangential fields at the first boundary and the second boundary,

Table 2 Performance characteristics of SPR sensor reflectance for diverse structures

Sensor structure used	R_{min}	Sensitivity (°RIU^{-1})	FWHM (°)	DA (°$^{-1}$)	QF (RIU^{-1})
BK7/Cu/sensing medium	0.6182	108	2.06	0.2621	52.42
BK7/Cu/TiO_2 /sensing medium	0.6269	146	4.22	0.1729	34.59
BK7/Cu/TiO_2/Ni/sensing medium	0.1652	324	5.31	0.3050	61.01
BK7/Cu(35 nm)/TiO_2(4*2 nm)/ Ni(10 nm)/BP(0.53 nm)/ sensing medium	0.0036	518	5.66	0.4575	91.51
BK7/Cu(35 nm)/TiO_2(2*2 nm)/ Ni(15 nm)/BP(0.53 nm)/ sensing medium	0.0832	526	5.45	0.4825	96.51

respectively, are M_1 and $M_{N—1}$. The individual matrix (Gj) for j-layer is offered by

$$G_j = \begin{bmatrix} \cos(T_j) & -\frac{i\sin(T_j)}{S_j} \\ -iS_j\sin(T_j) & \cos(T_j) \end{bmatrix} \quad (3)$$

Tj is the phase shift when the input light passes through the sheet.

$$T_j = \frac{2\pi}{\lambda} d(\varepsilon_j - (n_1 \sin\theta_1)^2)^{1/2} \quad (4)$$

where ε_j and dj are the jth material's dielectric constant and thickness, respectively.

For TM waves, $S_j = (\varepsilon_j - (n_1 \sin\theta_1)^2)^{1/2}/\varepsilon_j$. The structure's entire transfer matrix G can be written as

$$G = G_1G_2G_3G_4 = \begin{bmatrix} g_{11} & g_{12} \\ g_{21} & g_{22} \end{bmatrix} \quad (5)$$

where $G_1G_2G_3 and G_4$ are the matrices of the Cu, TiO_2, Ni and BP layers. Then, the reflectance (R) can be exemplified as

$$R = \left| \frac{(g_{11} + g_{12}S_N)S_1 - (g_{21} + g_{22}S_N)}{(g_{11} + g_{12}D_N)S_1 + (g_{21} + g_{22}S_N)} \right|^2 \quad (6)$$

Performance Parameters

The efficiency of surface plasmon resonance (SPR) sensors is commonly evaluated using parameters such as sensitivity (S), full width at half maximum (FWHM), detection accuracy (DA), quality factor (QF), and figure of merit (FoM) [42]. Sensitivity is a critical metric that reflects how the SPR sensor responds to changes in the refractive index (Δn) of the sensing medium, which induces a shift in the resonance angle ($\Delta\theta_{res}$). Sensitivity (S) is defined mathematically as [43]:

$$S\frac{\triangle\theta_{res}}{\triangle n} \quad (7)$$

The FWHM can also be determined from reflectance curve. It can be calculated as [44]:

$$FWHM = \theta_2 - \theta_1 \quad (8)$$

where θ_1 and θ_2 are the resonance angles at 50% reflectance measured from the resonance curve.

Detection accuracy (DA) can be obtained as [45, 46].

$$DA = \frac{\triangle\theta_{res}}{FWHM} \quad (9)$$

While the quality factor can be calculated as [47].

$$QF = S/FWHM \quad (10)$$

The figure of merit (FoM) is the product of the sensitivity and the detection accuracy of the sensor [48, 49]:

$$FoM = S \times DA \quad (11)$$

Results and Discussion

Comparison of the Current Sensor to Other Existing WorksO_2, Ni and BP in Kretschmann Configuration

Table 2 summarizes the performance metrics of the surface plasmon resonance (SPR) sensor as a function of the incident angle at various refractive indices (RI) of the sensing medium for different structural configurations. The variation in the sensor's reflectance spectrum with respect to the incident angle is illustrated in Fig. 2. For the conventional BK7/Cu/sensing medium configuration, Fig. 2a demonstrates a resonance dip shift of approximately 0.54° with a minimum reflection of 0.6182. The corresponding sensitivity is calculated to be 108°/RIU, with a quality factor (QF) of 52.42/RIU.

Incorporating an 8 nm TiO_2 layer into the SPR sensor structure (Fig. 2b) results in an upward shift of the resonance angle to 0.73°, along with a minimum reflection of 0.6269. The sensitivity is enhanced to 146°/RIU, although the QF decreases to 34.59/RIU. Further optimization by introducing

a 10 nm Ni layer alongside the TiO_2 layer (Fig. 2c) produces a resonance angle shift of 1.62°, with a significantly reduced minimum reflection of 0.1652. This configuration achieves a sensitivity of 324°/RIU and an improved QF of 61.01/RIU. Incorporating additional layers of black phosphorus (BP) into the structure (BK7/Cu/TiO_2 = 8 nm/Ni = 10 nm/BP) leads to a pronounced shift in the resonance angle to 2.59° and a remarkably low minimum reflection of 0.0036 (Fig. 2d). The sensitivity and QF for this configuration reach 518°/RIU and 91.51/RIU, respectively. A comparative analysis of structures with varying thicknesses of TiO_2 and Ni (BK7/Cu/TiO_2 = 8 nm/Ni = 10 nm/BP vs. BK7/Cu/TiO_2 = 4 nm/Ni = 15 nm/BP) reveals that the latter configuration achieves a slightly higher resonance angle of 2.63° with a minimum reflection of 0.00832. The sensitivity and QF values for this structure are further improved to 526°/RIU and 96.51/RIU, respectively.

The results clearly demonstrate that adding TiO_2, Ni, and BP layers to the Kretschmann configuration significantly enhances both the sensitivity and QF of the SPR sensor. A detailed comparative analysis of the results is presented in Table 3, highlighting the superiority of the optimized multilayered structures for advanced sensing applications.

Impact of $TiO_2$and Ni Thickness on Sensitivity and QF

The effects of TiO_2 and Ni layers on copper were systematically studied to determine the optimal thicknesses for maximizing sensor performance. Figure 3 presents the relationship between sensitivity, quality factor (QF), and variations in copper thickness (25–65 nm) and TiO_2 thickness (2–8 nm). Notably, Fig. 3a demonstrates an increase in sensitivity as both Cu and TiO_2 thicknesses increase, with the Ni layer fixed at 5 nm. For the adhesive sandwich structure, where the Ni layer is positioned between TiO_2 and BP, Ni thicknesses of 5 nm, 10 nm, and 15 nm were analyzed. The highest sensitivities were achieved with TiO_2 thicknesses of 8 nm and 4 nm, corresponding to 518°/RIU and 526°/RIU, respectively, for Ni thicknesses of 10 nm and 15 nm. These results are illustrated in Fig. 3b, c. In terms of QF, the optimal values were observed at Ni thicknesses of 5 nm and 15 nm, combined with a TiO_2 thickness of 2 nm, yielding QF values of 225.71/RIU and 136.89/RIU, respectively Fig. 3d, e. This indicates that both the Ni and TiO_2 layers effectively act as absorptive media, enabling efficient energy transfer to the copper film.

Additionally, Table 3 summarizes the minimum reflectance (Rmin) values for the analyzed structures, which are 0.0036 and 0.0832. As minimizing Rmin is a key design priority, the results underscore that a copper layer thickness of 35 nm is sufficient to achieve maximum sensor sensitivity. Consequently, the configuration BK7/Cu(35 nm)/TiO_2(4 × 2 nm)/Ni(10 nm)/BP(0.53 nm)/sensing medium was selected for subsequent simulations.

Effects of Ni Thickness and TiO_2 on Detection Accuracy(DA) and Figure of Merit

In order to improve the suggested SPR's performance, we experimented with several copper and nickel thickness

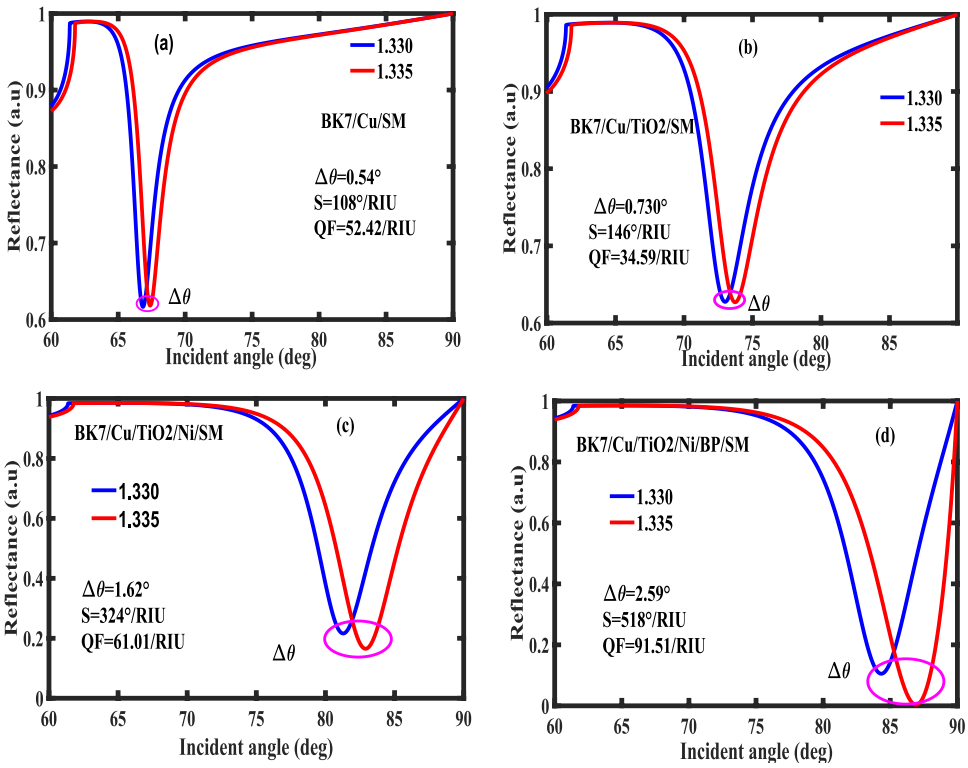

Fig. 2 Reflectance spectra for various structures of SPR sensor: BK7/Cu/SM (**a**), BK7/Cu/TiO_2/SM (**b**), BK7/Cu/TiO_2/Ni/SM (**c**), and BK7/Cu/TiO_2/Ni/BP/SM (**d**)

Table 3 Performance metric for the suggested SPR combination that is optimized

d(*Cu*)	d(*Ni*)	d(TiO_2)	R_{min}	S	FWHM	DA	QF
65	5	2	0.2729	158	0.70	1.128	225.71
65	10	2*3	0.6605	444	3.00	0.74	148
35	10	2*4	0.0036	518	5.66	0.4575	91.51
45	15	2	0.131	446	4.14	0.541	107.72
65	15	2	0.798	512	3.74	0.686	136.89
35	15	2*2	0.083	526	5.45	0.482	96.51
65	5	2*3	0.3165	216	1.16	0.931	186.2

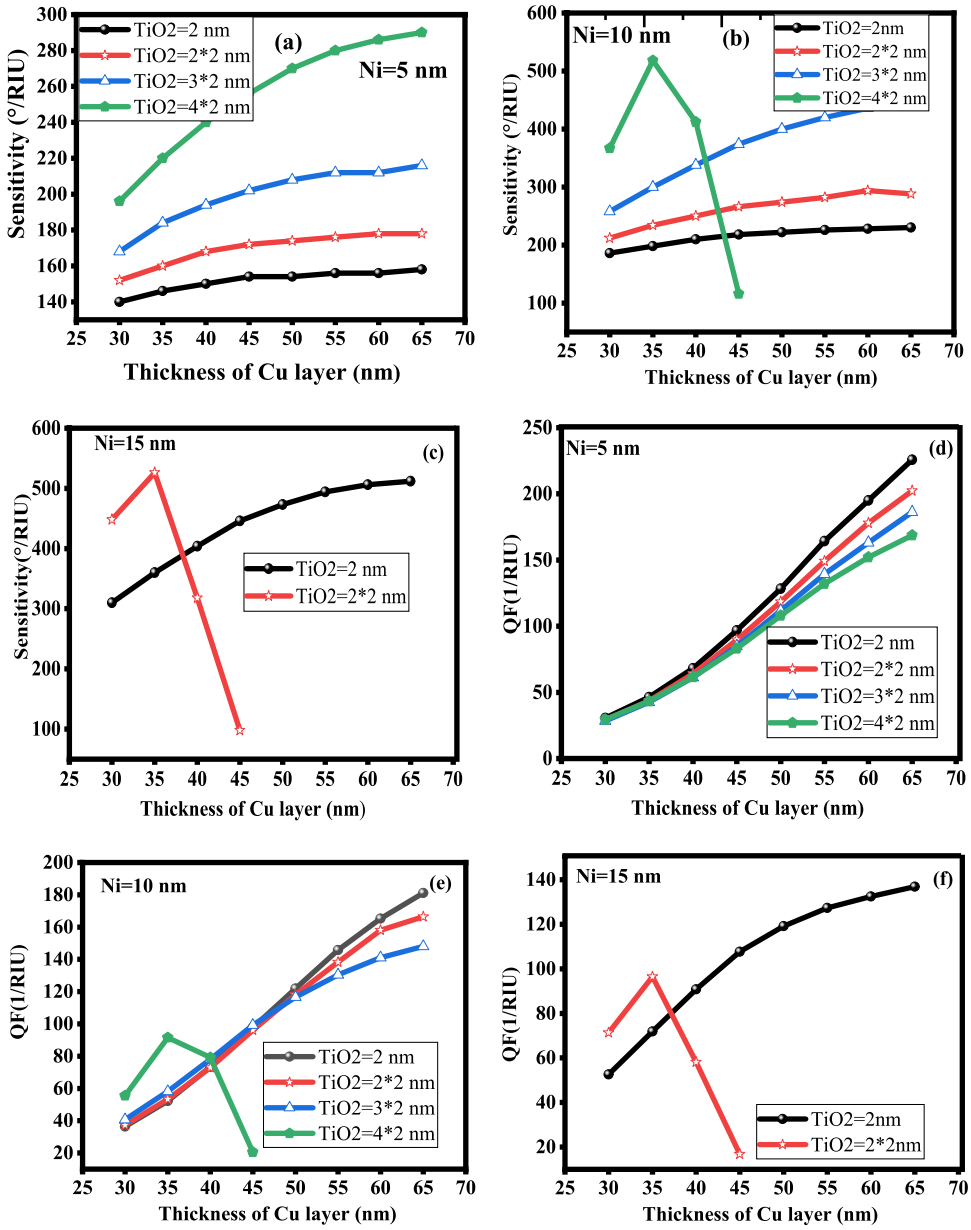

Fig. 3 Sensitivity and QF versus thickness of Cu layer. **a** TiO_2(2 to 8) nm for Ni = 5 nm. **b** TiO_2 (2 to 8) nm for Ni = 10 nm. **c** TiO_2 (2 to 4). **d** TiO_2 (2 to 8) nm for Ni = 5 nm. **e** TiO_2 (2 to 8) nm for Ni = 10 nm. **f** TiO_2 (2 to 4) for Ni = 15 nm

combinations for various TiO_2 layers. DA and FoM are computed for every combination of copper thickness (35, 40, 45, 50, 55, 60, 65 nm) and nickel layer thickness (5, 10, 15, 15 nm) for TiO_2 layers that are 2 nm to 8 nm thick.

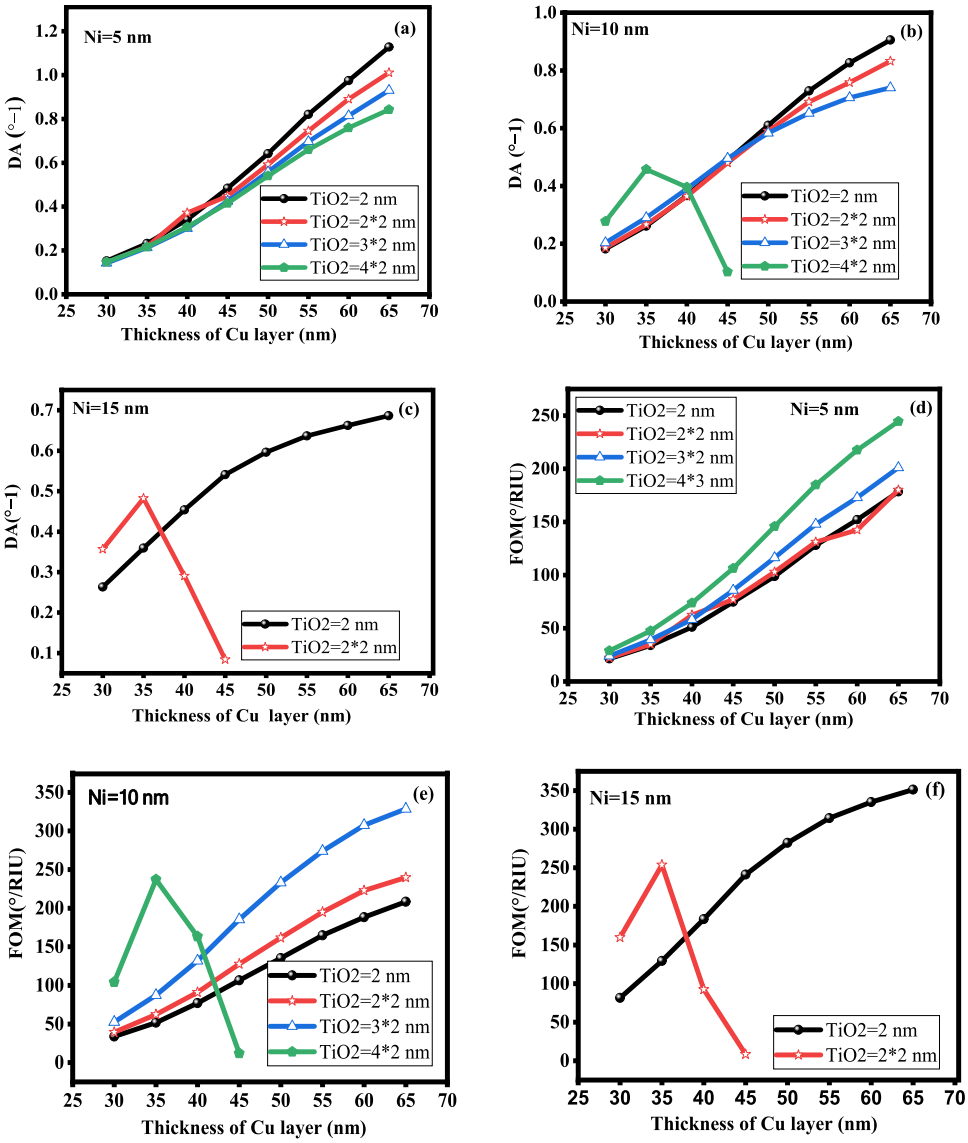

Fig. 4 DA and FoM versus thickness of Cu layer. **a** TiO_2 (2 to 8) nm for Ni = 5 nm. **b** TiO_2 (2 to 8) nm for Ni = 10 nm. **c** TiO_2 (2 to 4). **d** TiO_2 (2 to 8) nm for Ni = 5 nm. **e** TiO_2(2 to 8) nm for Ni = 10 nm. **f** TiO_2(2 to 4) for Ni = 15 nm

The change of detection accuracy (DA) and figure of merit (FoM) for varying numbers of TiO_2 layers (2*L) at varying copper layer thicknesses (35 nm to 65 nm) and nickel layer thicknesses (5 nm, 10 nm, and 15 nm) is shown in Fig. 4a–f. It was shown that as copper thickness increased, DA increased as well, and when Ni thickness and TiO_2 number increased, DA decreased.

The comparable variation DA in a traditional SPR sensor is shown in Fig. 4a–c as 1.1128/°, 0.9055/°, and 0.686/° with different structural thicknesses: corresponding to BK7/Cu(65 nm)/TiO_2(2 nm)/Ni(5 nm)/BP(0.53 nm)/SM; BK7/Cu(65 nm)/TiO_2(2 nm)/Ni(10 nm)/BP(0.53 nm)/SM; and BK7/Cu(65 nm)/TiO^2(2 nm)/Ni(15 nm)/BP(0.53 nm)/SM. When Ni increases, DA decreases because of the large imaginary value of Ni's dielectric constant, which dampens the effect of increased electron loss. Likewise, the FoM values for the following configurations are 244.47°/RIU, 328.56°/RIU, and 351.38°/RIU, respectively: BK7/Cu(65 nm)/TiO_2(2 nm)/Ni(5 nm)/BP(0.53 nm)/SM; BK7/Cu(65 nm)/TiO_2(2 nm)/Ni(10 nm)/BP(0.53 nm)/SM; and BK7/Cu(65 nm)/TiO_2(2 nm)/Ni(15 nm)/BP(0.53 nm)/SM. The suggested structure SPR sensor is seen to have a greater sensitivity and QF with minimal degradation and an increase in detection accuracy and FoM.

To enhance the performance of the proposed SPR sensor, we systematically experimented with various combinations of copper and nickel thicknesses across multiple TiO_2 layer configurations. Detection accuracy (DA) and the figure of merit (FoM) were calculated for each combination, with copper thicknesses ranging from 35 to 65 nm and nickel layer thicknesses of 5 nm, 10 nm, and 15 nm, for TiO_2 layers varying from 2 to 8 nm. Figure 4a–f illustrates the variations in DA and FoM for different numbers of TiO_2 layers (2 × L) across the specified copper and nickel thicknesses.

The results indicate that DA improves as copper thickness increases, while increasing the number of TiO_2 layers or Ni thickness causes a decrease in DA. This trend can be attributed to the large imaginary part of Ni's dielectric constant, which amplifies electron loss and dampens DA as the Ni thickness increases. The corresponding DA values for a traditional SPR sensor are presented in Fig. 4a–c: 1.1128°/°, 0.9055°/°, and 0.686°/°, corresponding to the structural configurations BK7/Cu(65 nm)/TiO_2(2 nm)/Ni(5 nm)/BP(0.53 nm)/SM, BK7/Cu(65 nm)/TiO_2(2 nm)/Ni(10 nm)/BP(0.53 nm)/SM, and BK7/Cu(65 nm)/TiO_2(2 nm)/Ni(15 nm)/BP(0.53 nm)/SM, respectively.

Similarly, the FoM values for these configurations are as follows: 244.47°/RIU, 328.56°/RIU, and 351.38°/RIU. The decrease in DA with increasing Ni thickness can be explained by the enhanced damping effect caused by the higher imaginary component of Ni's dielectric constant, leading to increased electron energy losses. The results demonstrate that the proposed SPR sensor structure offers higher sensitivity and QF while maintaining minimal performance degradation. The optimized configuration also yields improved detection accuracy and FoM, solidifying its potential as an advanced sensor design for precision applications.

The variation in FoM, DA, and QF with Cu thickness, as well as the thickness of the TiO_2 and Ni layer at 5 nm, 10 nm, and 15 nm, are displayed in Fig. 4.

Remarkably, Table 4 presents a comparative analysis between a subset of current SPR sensors and previously recommended works, showing that the current work improves performance with respect to both sensitivity and FoM.

Table 4 Comparison of the current sensor to other existing works

Ref	Year	Structure	S	DA	QF
[50]	2021	BK7/Cu/Ni/BP/Ti3C2Tx	304.47	0.174	60.52
[18]	2022	TiO_2/BP/Au–Ag-Cu	378	—	—
[51]	2023	$BaTiO_3$/WS_2/Al-Ni	400	—	—
[52]	2024	BK7/Cr/Au/Si/Graphene/WSe	333.33	0.588	196
[53]	2024	BK7/TiO_2/Cu/Fe2O3	406	0.1923	78.07
[54]	2024	BAK1/Ag/WS2/Ni/BP	198.15	–	64.79
[55]	2024	BAF10/Cu/KSnl3/Si	348.75	0.31	108.11
[56]	2024	BK7/Cu/$FASnI_3$/BP	459.22	0.2732	123.11
[57]	2024	CsF/Cu/Ni	426	–	–
Our study	–	BK7/Cu/TiO_2/Ni/BP	518	0.4575	91.51

Conclusion

This paper investigates a novel SPR sensor based on the Kretschmann configuration with high sensitivity uses the metal plasmonic copper Cu, TiO_2, Ni, and 2D materials (BP). The principal followed in this work is the attenuation total reflection method. Fresnel equations and the transfer matrix method computation has been by employed to theoretically analyze and examination of the reflection. The different designs of the SPR sensor were considered for optimal performance. It has furthermore been utilized for optimizing not just the angular sensitivity but also other sensor parameters including layer thickness and number. Optimization of TiO_2 and Nickel thickness to achieve the desirable Rmin and maximum sensitivity. Based on our simulations, we have found that the structure BK7/Cu/TiO_2/Ni/BP is more sensitive when 2D materials are added. The main performance parameter of our suggested SPR, which we attained with a 518°/RIU achievement and a FoM as high as 91.51/RIU, was structured by BK7/Cu(35 nm)/TiO_2(4*2 nm)/Ni(10 nM)/BP(0.53 nm) in the sensing medium's refractive index varying from 1.330 to 1.335. Where the highest sensitivity 526°/RIU can be obtained for copper (60 nm), TiO_2(4*2 nm), Ni(10 nm) and BP (0.53 nm). Additionally, the maximum quality factor (QF) is 96.51/RUI. The obtained results indicate that the suggested sensor yields more sensitive results than those reported in earlier studies. According to our findings, adding TiO_2, Ni, and 2D material to SPR sensors greatly increased their sensitivity and FoM for a variety of sensing uses in biosensing and diagnostics.

Acknowledgements The work was supported by Researchers Supporting Project number (RSP2025663), King Saud university, Riyadh, Saudi Arabia.

Author Contribution Conceptualization: H. Bouandas, A. Djemli Data curation: Y. Slimani Formal analysis: Malek G. Daher Methodology: Mika Sillanpää Writing and review & editing: Samar A. Aldossari Validation: M. Fatmi.

Funding Not applicable.

Data Availability Although the data supporting the findings in this study are not currently publicly available, they can be acquired upon reasonable request from the authors (fatmimessaoud@yahoo.fr).

Declarations

Conflicts of Interest The authors declare no competing interests.

References

1. Raghuwanshi SK, Pandey PS (2022) IEEE Trans Nanobiosci 22:292–300
2. Ansari G, Pal A, Sharma K, Srivastava AK, Verma G (2024) J Mater Res
3. Ansari G, Pal A, Srivastava AK, Verma G (2024) J Mater Res 39:1977–1988
4. Ansari G, Pal A, Srivastava AK, Verma G (2023) Sens Bio-Sens Res 42:00605

5. Ansari G, Pal A, Srivastava AK, Verma G (2023) Opt Laser Technol 164:109495
6. Karki B, Uniyal A, Sharma M, Yadav RB, Buduma P (2024) J Comput Electron: 1–10
7. Otto A (1968) Z Phys 216:398–410
8. Elsayed HA, Awasthi SK, Almawgani AHM, Mehaney A, Ali YAA, Alzahrani A, Ahmed AM (2024) RSC Adv 14:7877
9. Maier SA (2007) Springer Science, Business Media
10. Reather H (1988) Springer tracts in modern physics, vol 111. pp 1–3
11. Kumar R, Singh S, Bouandas H, Alam J (2025) Plasmonics 1–11:1557–1963
12. West PR, Ishii S, Naik GV, Emani NK, Shalaev VM, Boltasseva A (2010) Laser Photonics Rev 4(6):795–808. Springer
13. Singh Raman RK, Chakraborty Banerjee P, Lobo DE, Gullapalli H, Sumandasa M, Kumar A, Choudhary L, Tkacz R, Ajayan PM, Majumder M (2012) Carbon 50(11):4040–4045
14. Karki B, Uniyal A, Pal A, Srivastava V (2022) Int J Optics: 1476254
15. Karki B, Vasudevan B, Uniyal A, Pal A, Srivastava V (2022) 270:169947
16. Karki B, Trabelsi Y, Pal A, Taya SA, Yadav RB (2024) Opt Mater 147:114555
17. Karki B, Pal A, Sarkar P, Yadav RB, Muduli A, Trabelsi Y (2024) Silicon 16:3861–3872
18. Karki B, Pal A, Singh Y, Sharma S (2022) Opt Commun 508:127616
19. Karki B, Sarkar P, Mahmoud KH, Alsubaie ASA, Sharma M (2024) Plasmonics
20. Karki B, Alsubaie AS, Sarkar P, Sharma M, Ben Ali N (2024) Plasmonics
21. Karki B, Pal A, Saad Alsubaie A, Mahmoud KH, Sharma M (2024) Phys B: Condens Matter 695:416503
22. AlaguVibisha G, Nayak JK, Maheswari P, Priyadharsini N, Nisha A, Jaroszewicz Z, Rajesh K, Jha R (2020) Opt Commun 463:125337
23. Cho SY, Cho SY, Lee Y, Koh H, Jung H, Kim J, Yoo H, Kim J, Junget H (2016) Adv Mater 28(32):7020–7028
24. Mao N, Tang J, Xie L, Wu J, Han B, Lin J, Deng S, Ji W, Xu H, Liu K, Tong L, Zhang J (2016) Am Chem Soc 138:300–305
25. Wu L, Guo J, Wang Q, Lu S, Dai X, Xiang Y, Fan D (2017) Sens Actuators B: Chem 249:542–548
26. Kumar R, Trabelsi Y, Garia L, Kakar VK, Pal A (2024) Chem Mater Sci Eng Phys Scr 27
27. Kumar R, Singh MK, Garia L, Patel BD (2024) Plasmonics 19(1):203–213
28. Mudgal N, Saharia A, Choure KK, Agarwal A, Singh G (2020) Appl Phys A 126(12):1–8
29. Xu ZJ, Zhang F, Zhang RJ, Yu X, Zhang DX, Wang ZY, Zhao HB, Chen LY (2013) Appl Phys A 113:557–562
30. Gao D, Guan C, Wen Y, Zhong X, Yuan L (2014) Opt Commun 313:94–98
31. Zhang H, Chen Y, Wang H, Hu S, Xia K, Xiong X, Huang W, Lu H, Yu J, Guan H, He M, Liu W, Zhang J, Luo Y, Xie Z, Chen Z (2018) Opt Express 26:33226–33237
32. Mostufa S, Akib TBA, Rana MM, Islam MR (2022) Biosensors 12(8):603
33. Guo S, Wu X, Li Z, Tong K (2020) Int J Opt 2020
34. Singh S, Upadhyay A, Chaudhary B, Sirohi K, Kumar S (2023) IEEE Sens J
35. Moznuzzaman M, Khan I, Islam MR (2021) AIP Adv 11(6):1–10
36. Vibisha GA, Daher MG, Rahman SH, Jaroszewicz Z, Rajesh K, Jha R (2023) Results Opt 11
37. AlaguVibisha G, Nayak JK, Maheswari P, Priyadharsini N, Nisha A, Jaroszewicz Z, Jha R (2020) Opt Commun 463:125337
38. Fox M (2010) Optical properties of solids. Oxford University Press
39. Moznuzzaman M, Khan I, Islam MR (2021) AIP Adv 11
40. Peng Q, Wang Z, Sa B, Wu B, Sun Z (2016) Sci Rep 6:1–10
41. Malek GD (2023) Optik 275:170581
42. Bouandas H, Chorfi H, Ayadi K (2021) Optik 225:165809
43. Daher MG, Trabelsi Y, Prajapati YK, Panda A, Ahmed NM, Rashed ANZ (2023) Opt Quant Electron 55:199
44. Daher MG, Taya SA, Almawgani AH, Hindi AT, Colak I, Patel SK (2023) Plasmonics 18(6):2195–2204
45. Daher MG, Ahmed NM, Alsalman O, Panda A, Rashed ANZ, Parmar J, Taya SA, Patel SK (2023) Plasmonics 18(6):2069–2075
46. Bouandas H, Slimani Y, Ayadi K, Ghebouli MA, Djemli A, Fatmi M, Chihi T, Albaqami MD, Mohammad S, Sillanpaa M (2024) J Opt: 1–9
47. Daher MG, Trabelsi Y, Ahmed NM, Prajapati YK, Rashed ANZ, Patel SK (2023) Plasmonics 18(6):2483–2492
48. Daher MG, Ahmed NM, Patel SK, Al-Zahrani FA (2023) Opt Quant Electron 55(12):1102
49. Bouandas H, Slimani Y, Faisal Katib Alanazi, Fatmi M, Chihi T, Djemli A (2024) J Opt: 1-8
50. Setareh M, Kaatuzian H (2021) Superlattices Microstruct 153:106867
51. Mohd U, Bijalwan A, Rastogi V (2023) Phys Scr 98(10):105515
52. Salehnezhad Z, Soroosh M, Mondal H (2024) Photonics 11(6)
53. Muthumanikkam M, Vibisha A, Lordwin Prabhakar MC, Suresh P, Rajesh KB, Jaroszewicz Z, Jha R (2023) Sensors 23(17):7495
54. Kumar R, Singh S, Chaudhary B, Kumar S (2024) IEEE Trans Plasma Sci
55. Kumar R, Trabelsi Y, Garia L, Kakar VK, Pal A (2024) Phys Scr 99(9):095543
56. Bouandas H, Slimani Y, Bakhouche A, Bioud N, Djemli A, Faisal Katib Alanazi, Bouchama I, Ghebouli MA, Fatmi M, Chihi T (2024) Results Phys 66:108004
57. Alagu Vibisha G, Nayak JK, Maheswari P, Priyadharsini N, Nisha A, Jaroszewicz Z, Jha R (2020) Opt Commun 463:125337